JOURNAL OF VIROLOGY, Sept. 2009, p. 8744–8758 Vol. 83, No. 17
0022-538X/09/$08.00+0 doi:10.1128/JVI.00613-09

Proteolytic Activation of the Spike Protein at a Novel RRRR/S Motif Is Implicated in Furin-Dependent Entry, Syncytium Formation, and Infectivity of Coronavirus Infectious Bronchitis Virus in Cultured Cells[▽]

Yoshiyuki Yamada[1] and Ding Xiang Liu[1,2]*

Institute of Molecular and Cell Biology, 61 Biopolis Drive, Proteos, Singapore 138673,[1] and Department of Biological Sciences, National University of Singapore, Science Drive 4, Singapore 117543[2]

Received 25 March 2009/Accepted 13 June 2009

The spike (S) protein of the coronavirus (CoV) infectious bronchitis virus (IBV) is cleaved into S1 and S2 subunits at the furin consensus motif $RRFRR_{537}$/S in virus-infected cells. In this study, we observe that the S2 subunit of the IBV Beaudette strain is additionally cleaved at the second furin site ($RRRR_{690}$/S) in cells expressing S constructs and in virus-infected cells. Detailed time course experiments showed that a peptide furin inhibitor, decanoyl-Arg-Val-Lys-Arg-chloromethylketone, blocked both viral entry and syncytium formation. Site-directed mutagenesis studies revealed that the S1/S2 cleavage by furin was not necessary for, but could promote, syncytium formation by and infectivity of IBV in Vero cells. In contrast, the second site is involved in the furin dependence of viral entry and syncytium formation. Mutations of the second site from furin-cleavable RRRR/S to non-furin-cleavable PRRRS and AAARS, respectively, abrogated the furin dependence of IBV entry. Instead, a yet-to-be-identified serine protease(s) was involved, as revealed by protease inhibitor studies. Furthermore, sequence analysis of CoV S proteins by multiple alignments showed conservation of an XXXR/S motif, cleavable by either furin or other trypsin-like proteases, at a position equivalent to the second IBV furin site. Taken together, these results suggest that proteolysis at a novel XXXR/S motif in the S2 subunit might be a common mechanism for the entry of CoV into cells.

The surface glycoproteins of numerous pathogenic enveloped viruses are proteolytically matured during infection in the host or cultured cell lines and are essential for the initiation of infection (33). In many cases, this processing is carried out by cellular proprotein convertases (PCs), most commonly furin (reviewed in reference 46). Furin is a calcium-dependent serine protease that circulates between the *trans*-Golgi network, plasma membrane, and early endosome by association with exocytic and endocytic pathways (9, 39). This membrane-bound enzyme undergoes further processing and is secreted from cells in an active soluble form (49). Furin processes a wide variety of precursor proteins after the C-terminal arginine (R) residue in the preferred consensus motif RXR(K)R/X (K is lysine, X is any amino acid, and the slash [/] indicates the cleavage position) for viral fusion proteins (2, 32, 33). So far, seven PCs have been identified in mammalian cells, and they display similar, but not identical, specificities for basic motifs at the cleavage site of a substrate. Accumulated studies indicate that secretory PCs, such as furin, PC5, and PC7, are major candidates for processing surface glycoproteins of pathogenic viruses, such as human immunodeficiency virus types 1 and 2, avian influenza virus H5N1, Ebola virus, and respiratory syncytial virus (RSV) (2, 27).

Coronavirus (CoV) spike (S) protein, a class I viral fusion protein (7), is responsible for viral attachment to and entry into target cells and for cell-to-cell spread during infection. Typical class I fusion proteins usually require processing at a position immediately upstream of the fusion peptide in order to expose the membrane-anchored subunit. However, in infectious bronchitis virus (IBV) and murine hepatitis virus (MHV), processing of the S protein by furin occurs at a position more than 200 amino acids away from the predicted fusion peptides (6). Furthermore, there is a tradeoff between the furin cleavability of S protein and heparin sulfate (HS) binding in certain CoV strains adapted to cultured cell lines (15, 17). Consequently, CoV S proteins may be proteolytically activated by other proteases to initiate virus-cell fusion. Recently, proteolytic activation by an endosomal protease, cathepsin L, and a membrane-bound protease, factor Xa, was reported to play a role in the entry of severe acute respiratory syndrome (SARS)-CoV (18, 45). Cathepsin is also implicated in the proteolytic activation of many CoV S proteins, including human CoV 229E, feline infectious peritonitis virus (FIPV) 1146, feline enteric CoV (FECV) 1683, and MHV strain 2 (MHV-2), but not for MHV A59 and human CoV NL63 (31, 41, 43, 45).

The association of cell surface sialic acid and a low-pH environment were reported to be required for IBV entry (14, 51, 52). However, the factors that determine the infectivity of IBV for cultured cells have yet to be identified. Clinical and field isolates of IBV can be propagated only in embryonated chicken eggs or, transiently, in primary chicken embryo kidney cells. In contrast, IBV of Beaudette strain origin can be readily adapted to cultured cells, such as Vero and BHK-21, by serial passages (1, 22, 40), and hence, it is often used as an in vitro

* Corresponding author. Mailing address: Institute of Molecular and Cell Biology, 61 Biopolis Drive, Proteos, Singapore 138673. Phone: 65 6586 9581. Fax: 65 6779 1117. E-mail: dxliu@imcb.a-star.edu.sg.

▽ Published ahead of print on 24 June 2009.

infection model of IBV. Studies with a recombinant infectious clone system demonstrated that IBV S protein is indeed the determinant of extended cell tropism (12). IBV S protein is usually cleaved into S1 and S2 subunits at the furin consensus motif, $RRFRR_{537}$/S (the position includes the signal peptide) in virus-infected cells (13). Interestingly, Beaudette and related strains carry a mutation at position 687 of the S protein from proline (P) to R, creating a novel furin site ($RRRR_{690}$/S or $RRKR_{690}$/S). The acquisition of an additional furin site in the fusion protein may increase cell-to-cell spread by further activation of the protein (23) or extend the host range by utilization of cell surface HS as an entry receptor (17). In this study, furin-mediated cleavage of the IBV S protein at two furin sites was observed in IBV-infected cells. Mutational analysis of the two furin sites revealed that the second site is implicated in the furin dependence of IBV entry and syncytium formation. In contrast, cleavage at the S1/S2 site by furin was not necessary for, but could promote, syncytium formation and the infectivity of IBV in Vero cells.

MATERIALS AND METHODS

Cells and viruses. HuH-7 and Vero (ATCC CCL-81) cells were maintained in Dulbecco's modified Eagle's medium (DMEM) supplemented with 10% fetal bovine serum (FBS) in the presence of penicillin (100 units/ml) and streptomycin (100 μg/ml) at 37°C in a 5% CO_2 environment. The passage 65 (designated wild-type [WT] virus here) of Vero-adapted IBV Beaudette, the recombinant IBV (rIBV [WT]), and rIBV-Luc Δ3a3b (rIBV-Luc [expressing the luciferase gene]) were described before (21, 22, 44). The recombinant vaccinia/T7 virus and IBV strains were propagated in Vero cells, and the 50% tissue culture infective doses ($TCID_{50}$) of viral stocks were calculated by the Reed-Muench method (42). Viral stocks were kept at −80°C until they were used.

Chemicals and antibodies. 4-(2-Aminoethyl)benzenesulfonyl fluoride hydrochloride (AEBSF), leupeptin, and trypsin were purchased from Sigma Aldrich. Furin inhibitor (decanoyl-Arg-Val-Lys-Arg-chloromethylketone) was purchased from Calbiochem. The anti-IBV S polyclonal antibody (S2 Ab) was made by the immunization of rabbits with a truncated S protein (positions 387 to 687) and could recognize only the S2 subunit from amino acids 538 to 687, as confirmed by Western blotting (WB) and immunoprecipitation analysis of truncated S constructs (data not shown). Mouse monoclonal Abs against human β-tubulin and Flag epitope were purchased from Sigma Aldrich. The fluorescein isothiocyanate-conjugated anti-mouse and -rabbit immunoglobulin G (IgG) and horseradish peroxidase-conjugated anti-human, -mouse, and -rabbit IgG were purchased from Dako.

Plasmid construction and transfection. Plasmid pKT-0, which has a T7 promoter for transcription, was used for transient transfection (38). The pKT-S construct encoding the full-length S protein was previously reported (53). Epitope-tagged constructs were made by overlap PCR and cloned into pKT-0. Point mutations were made by site-directed mutagenesis using the Quikchange kit (Stratagene). Cells at about 90% confluence were infected with the recombinant vaccinia/T7 virus for 1 h, followed by transfection of plasmid DNA using the Effectene transfection reagent (Qiagen).

WB. Each sample was lysed with 1× sodium dodecyl sulfate (SDS) sample loading buffer without bromophenol blue, and the protein concentration was determined with the Bio-Rad Protein Assay kit. Equal amounts of total protein were separated by SDS-polyacrylamide gel electrophoresis and transferred to polyvinylidene difluoride membranes. The membranes were incubated with a primary Ab and subsequently with a horseradish peroxidase-conjugated secondary Ab and detected using the ECL Advance Western Blotting Detection Kit (Amersham).

IF staining. Vero cells were cultivated in four-well chamber slides (Iwaki). IBV-infected cells or plasmid-transfected cells were washed with phosphate-buffered saline (PBS) supplemented with 10% normal goat serum, fixed with 4% paraformaldehyde in PBS for 15 min, and permeabilized with 0.2% Triton X-100 for 10 min. Immunofluorescent (IF) staining was performed by incubating the cells with the S2 Ab and subsequently with fluorescein isothiocyanate-conjugated anti-rabbit IgG. The cells were examined by fluorescence microscopy.

Quantitative real-time reverse transcription (RT)-PCR. Total RNA was extracted from virus-infected cells by using Tri Reagent (Molecular Research Center, Inc.) and treated with DNase I. The RNA concentration was measured with an ND-1000 spectrophotometer (NanoDrop Technologies), and 2 μg of RNA was reverse transcribed with Expand Reverse Transcriptase (Roche). A primer combination of IBV4527(+) (5′-TTTAGCAGAACATTTTGACGCA GAT) and IBV4805(−) (5′-TTAGTAGAACCAACAAACACGACAG) was used for either positive- or negative-strand genomic RNA (gRNA) amplification. Real-time PCR was performed using the LightCycler FastStart DNA Master SYBR green I kit according to the manufacturer's instructions (Roche). PCR was carried out for 40 cycles at 95°C for 10 s, 57°C for 10 s, 72°C for 15 s, and 75°C for 1 s. The GAPDH (glyceraldehyde-3-phosphate dehydrogenase) mRNA level was also quantified to normalize the IBV gRNA level with a primer combination of GAPDH(RT) (5′-TCTACATGGCAACTGTGAGGA), GAPDH(+) (5′-GACAACTTTGGTATCGTGGAA), and GAPDH(−) (5′-CCAGGAAATGA GCTTGACA). PCR for GAPDH was carried out for 40 cycles at 95°C for 10 s, 55°C for 10 s, 72°C for 15 s, and 80°C for 1 s.

In vitro transcription of full-length IBV cDNA and electroporation. The detailed procedure to create a full-length IBV cDNA clone was previously reported (21). The S gene of the partial IBV cDNA was replaced with mutant S genes and subsequently ligated into full-length IBV cDNA. Full-length transcripts were generated in vitro using the mMessage mMachine T7 kit (Ambion, Austin, TX). IBV N gene transcripts were also generated to enhance the recovery of virus. Vero cells at about 90% confluence were trypsinized, washed twice with ice-cold PBS, and resuspended in PBS. RNA transcripts were introduced into Vero cell using the Bio-Rad Gene Pulser II electroporator. The cells were cultured overnight in 1% FBS-containing DMEM in a six-well plate and further incubated in DMEM without FBS. At 48 h postelectroporation, viral-RNA replication was investigated by RT-PCR of the negative-strand gRNA. Transcription of subgenomic mRNAs was investigated by RT-PCR as described previously (21). The S genes of the recovered rIBV clones (at the second passage in Vero cells) were amplified by RT-PCR and subsequently confirmed by DNA-sequencing analysis. Characterization was carried out with the third passage of viruses in Vero cells.

Treatment of cells with protease inhibitors. Monolayers of Vero cells in 12-well plates were pretreated with furin inhibitor or protease inhibitors for 1 h at 37°C and infected with 10^5 $TCID_{50}$ of rIBV for 2 h at 37°C (or 1 h at 4°C) in the presence of the agents. The cells were washed three times with PBS, and the medium was changed to fresh DMEM without agents (pretreatment). Posttreatment with furin inhibitor was carried out after virus infection (2 h at 37°C or 1 h at 4°C) by replacement of the culture media with fresh DMEM containing different concentrations of furin inhibitor, and the cells were incubated in the presence of the inhibitor. The cells were washed three times with PBS, and replication of the virus was investigated. The luciferase activity in rIBV-Luc-infected cells was measured with the Luciferase Assay System (Promega). Passive lysis buffer (Promega) was used for cell lysate preparation.

RESULTS

IBV S protein is cleaved by furin at both the $RRFRR^{537}$/S and $RRRR^{690}$/S positions. Prediction of a furin cleavage site on the ProP server (19) (http://www.cbs.dtu.dk/services/ProP/) showed the presence of an additional furin site at the ectodomain with either an $RRRR_{690}$/S or an $RRKR_{690}$/S motif in Beaudette and derivative strains of IBV (Fig. 1a). To determine if the RRRRS sequence is a furin substrate, a construct, S(1-789)Fc, covering the N-terminal 789-amino-acid region of the IBV S protein with a C-terminal Fc tag (Fig. 1a), was created and expressed in HuH-7, a cell line that cleaves the IBV S protein efficiently. In addition, two deletion constructs, Δ1 (Δ533-537) and Δ2 (Δ687-690), with deletion of the first and second furin sites, respectively, were created (Fig. 1a) and expressed. As shown in Fig. 1b, similar levels of S(1-789)Fc* (glycosylated forms are shown with asterisks) bands were detected from all constructs. The predicted C-terminal cleavage product from the first site (C terminus; cl-1C*) was detected as multiple bands in cells transfected with the WT and Δ2, but not with Δ1 (lanes 3 and 5), while the cleavage product from the second site (cl-2C*) was detected in cells expressing the WT and Δ1 (lanes 3 and 4). Interestingly, the cl-1C* species was weaker in cells expressing the WT S construct than in those

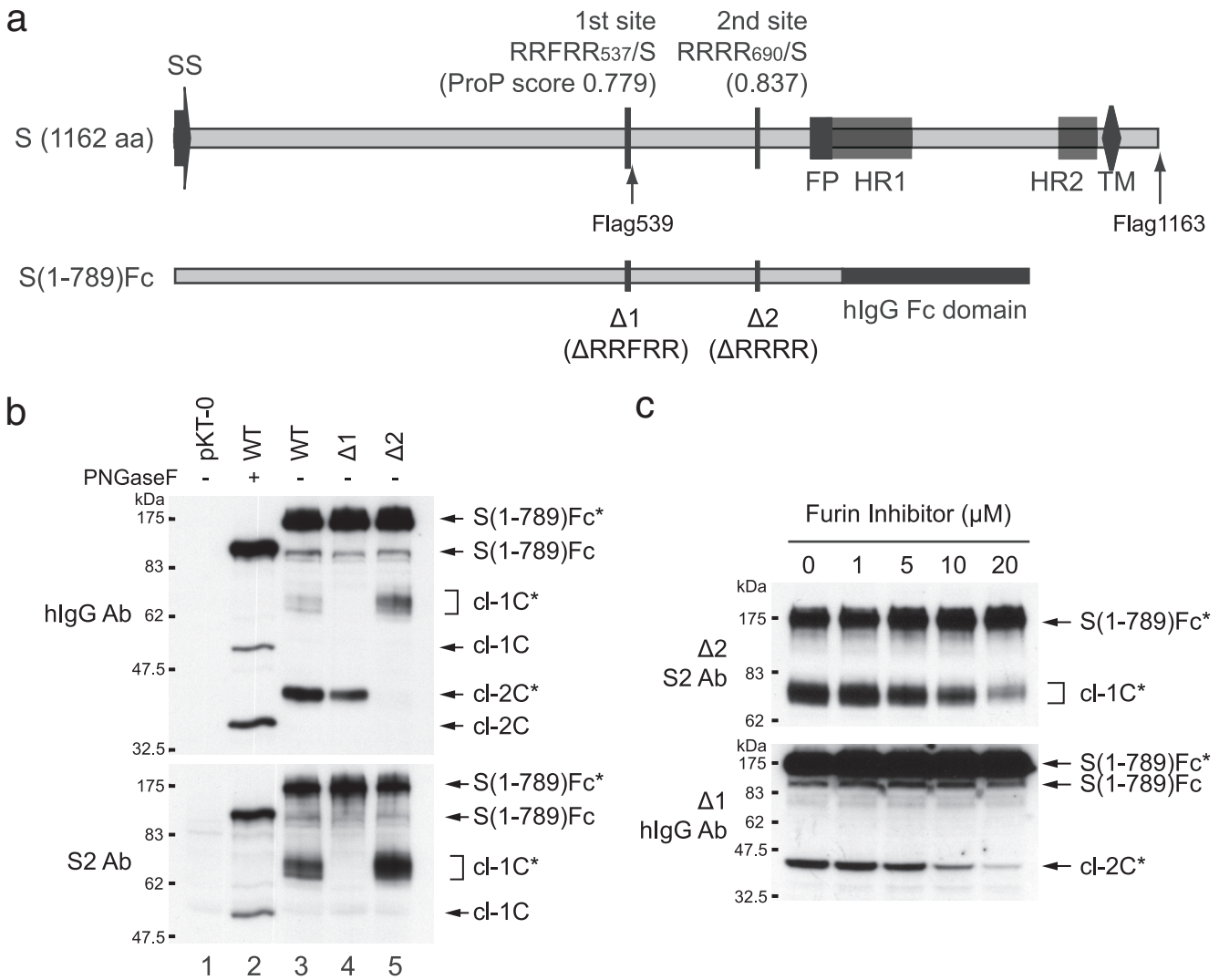

FIG. 1. An in vitro assay shows that $RRRR_{690}$/S of the IBV S protein is a furin substrate. (a) Schematic diagram of S protein from Vero-adapted IBV Beaudette and furin cleavage sites predicted by the ProP server. Constructs that encode full-length S and truncated S fused to the human IgG Fc domain, S(1-789)Fc, are illustrated. The positions for inserting the Flag tag, the putative signal sequence (SS), the fusion peptide (FP), heptad repeats 1 and 2 (HR1 and HR2), the transmembrane domain (TM), and the amino acid (aa) sequences deleted in the two deletion constructs (Δ1 and Δ2) are also shown. (b) Detection of cleavage at the two furin sites. The S(1-789)Fc constructs were expressed in HuH-7 cells for 24 h, total cell lysates were prepared, and PNGase F (New England Biotechnology) treatment was carried out for 2 h at 37°C. Cell extracts were analyzed by WB. (c) Inhibition of furin-dependent cleavage by furin inhibitor. At 6 h posttransfection of S(1-789)Fc constructs in HuH-7 cells, the culture media were replaced with fresh DMEM containing different concentrations of furin inhibitor. The cells were further incubated for 18 h, and cell extracts were analyzed by WB.

expressing Δ2 (Fig. 1b, lanes 3 and 5), probably due to further cleavage of the species at the second site in the WT S protein, as described below. Treatment of samples with PNGase F confirmed that the unglycosylated bands were consistent with the predicted molecular masses of full-length [S(1-789)Fc; 111.1 kDa] and cleaved products from the S1/S2 site (cl-1C; 52.3 kDa) and the second site (cl-2C; 35.1 kDa), respectively (lane 2). The predicted dual-cleavage product could be detected in cells expressing WT, but not mutant, S constructs in a 12% gel (data not shown). To further investigate if cleavage at these two sites was furin dependent, increasing concentrations of furin inhibitor were added to cells expressing Δ1 and Δ2. Both cl-1C* and cl-2C* decreased depending on the concentration of furin inhibitor, but S(1-789)Fc* was at a constant level (Fig. 1c).

Cleavage products at two furin sites are detected in IBV-infected cells. To facilitate the detection of S protein cleavage in IBV-infected cells, two rIBV clones with a Flag-tagged S gene were created. As shown in Fig. 1a, the Flag tag (underlined) was placed either immediately after the S1/S2 cleavage site (S-Flag539; -RRFRR/SMDYKDDDDKIF-) or the C terminus of the S protein (S-Flag1163; -RPKKSVMDYKDDDDK). Infection of cells with rIBV(S-Flag539) would be expected to detect the full-length S and S2 and the N-terminal cleavage product from the second site [cl-2N; S(1-690) or S(19-690)] and the dual-cleavage fragment [cl-

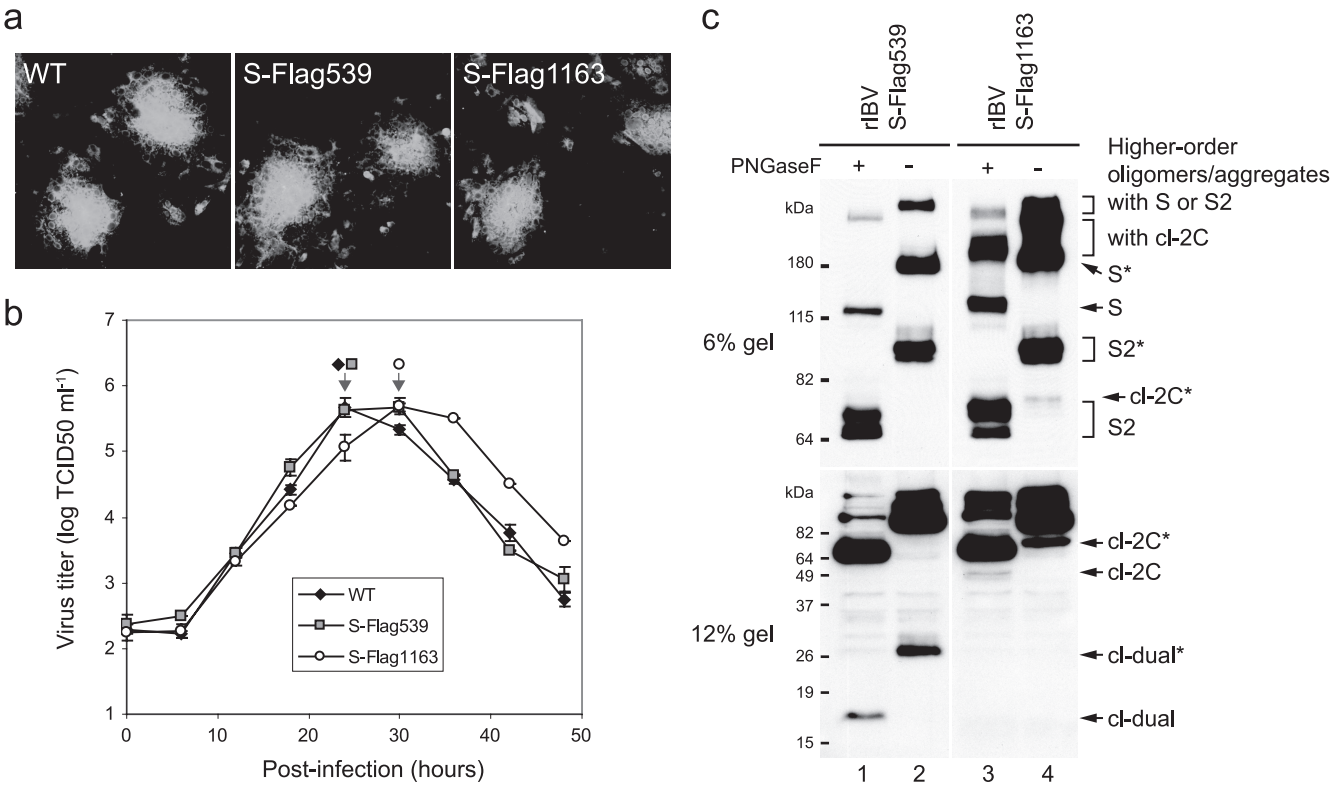

FIG. 2. Cleavage products at two furin sites are detected in IBV-infected cells. (a) Syncytium formation by rIBV was not affected by Flag-tagged S genes. Vero cells were infected with rIBV for 2 h. The cells were washed three times with PBS and incubated for 16 h with an overlay of DMEM containing 0.6% carboxymethyl cellulose. Syncytium formation was observed by IF staining with the S2 Ab. (b) Replication of S-Flag1163 was slightly delayed compared to the WT and S-Flag539. Vero cells (in a 25-cm^2 flask) were infected with rIBV and harvested at 0, 6, 12, 18, 24, 30, 36, 42, and 48 h postinfection. Viral stocks were prepared by freezing/thawing of the cells three times, and the $TCID_{50}$ was determined. The arrows indicate the time points when CPE was observed in nearly 100% of the cells. The error bars indicate standard errors of the means. (c) Cleavage at two furin sites was detected in virus-infected cells. HuH-7 cells were infected with rIBV for 18 h. Cell extracts were analyzed by WB with the anti-Flag Ab.

dual; S(538-690)]. Infection of cells with rIBV(S-Flag1163) would be expected to detect S, S2, and the C-terminal cleavage product from the second site [cl-2C; S(691-1162)]. Following electroporation of the in vitro-transcribed full-length RNA into Vero cells, infectious viruses were successfully recovered. Both S-Flag539 and S-Flag1163 viruses developed syncytia of a similar size to those of the WT (Fig. 2a). Analysis of the growth kinetics showed that the two rIBV clones propagated well in Vero cells, but the replication of S-Flag1163 was slightly delayed compared to the WT and S-Flag539 (Fig. 2b). These data indicated that insertion of Flag539 at a position immediately downstream of the S1/S2 cleavage site had minimal, if any, effect on the function of the S protein.

In cells infected with the two recombinant viruses, the glycosylated S (S*) and S2 (S2*) were detected in an SDS-6% polyacrylamide gel (Fig. 2c, top). Treatment of the samples with PNGase F efficiently removed the carbohydrate chains, leading to the detection of the unglycosylated S and S2 (Fig. 2c, top); S2 was still detected as double bands after the treatment (lanes 1 and 3). The predicted cleavage product at the second furin site ([S(691-1162)] was also detected in S-Flag1163-infected cells (lanes 3 and 4); however, its intensity was significantly reduced compared to S2. In addition, abundant bands migrating even more slowly than S and S* were detected (Fig. 2c). The identities of these bands are not clear, but they may represent higher-order oligomers/aggregates of the S protein. When samples were separated in an SDS-12% acrylamide gel, the predicted dual-cleavage fragment [S(538-690)] (lanes 1 and 2) was clearly detected. However, the putative intermediate cleavage products S(1-690)* and S(19-690)*, covering the N-terminal region up to the second furin site, were not detected in S-Flag539-infected cells (lanes 1 and 2).

Entry and syncytium formation by IBV are blocked by furin inhibitor. The effects of furin inhibitor on the attachment and entry of IBV were investigated by real-time RT-PCR optimized with specific primers on the 1a region. Pretreatment of Vero cells with different concentrations of furin inhibitor revealed that the attachment of WT virus was not affected at both 4 and 37°C, and no reduction in the positive-strand gRNAs was observed (Fig. 3a, 0 h). The effects of both pre- and posttreatment on IBV entry were evaluated at 4 h postinfection. The ratio between positive- and negative-strand gRNAs was approximately 50:1 in all samples. Interestingly, both positive- and negative-strand gRNAs were reduced by 40 to 60% by pretreatment (Fig. 3a, pretreatment at 4 h) but were only slightly decreased in posttreated cells (Fig. 3a, posttreatment at 4 h at 37°C). These data indicated that furin inhibitor blocked IBV entry with minimal effect on gRNA replication.

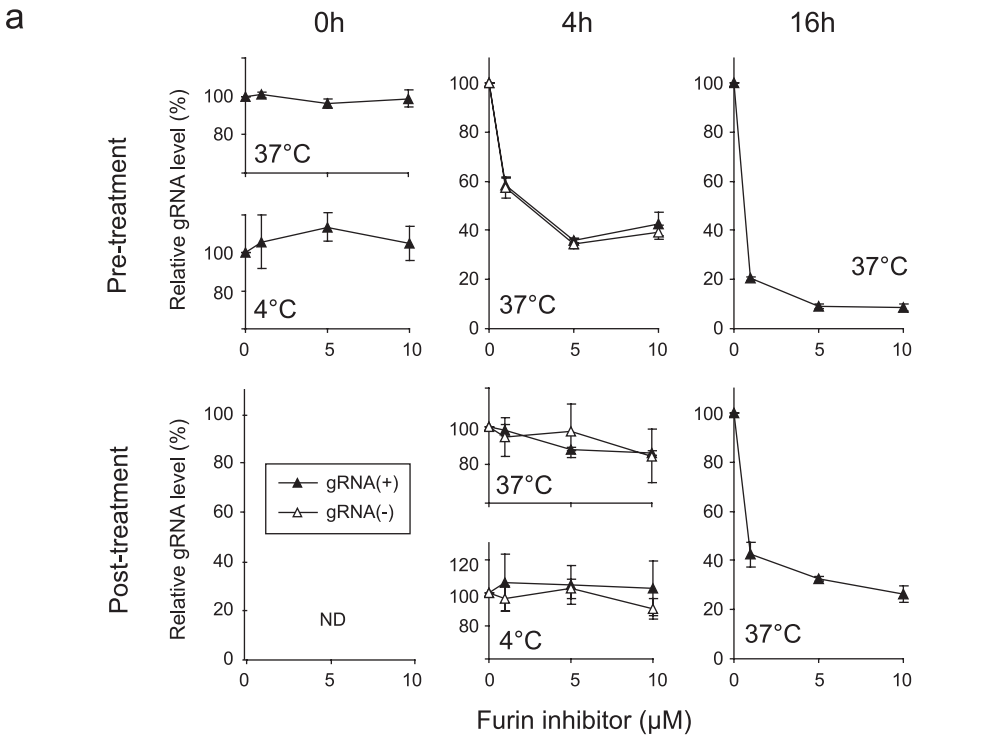

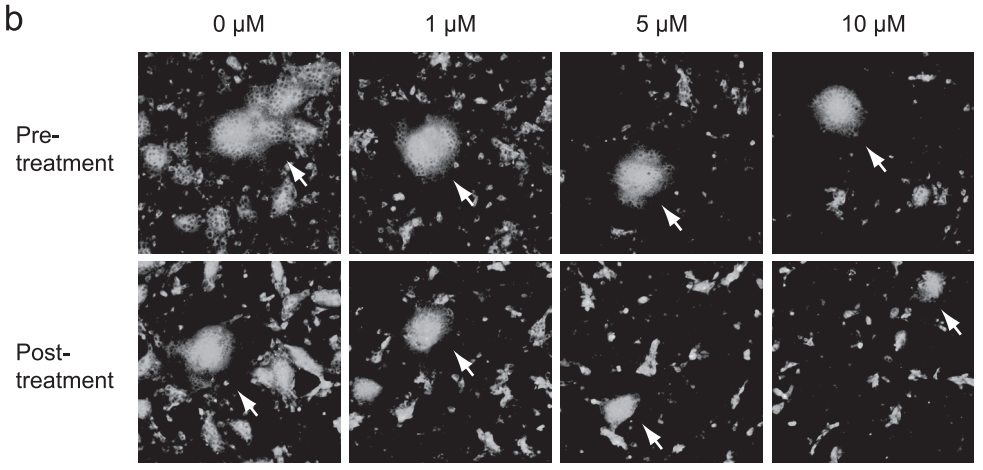

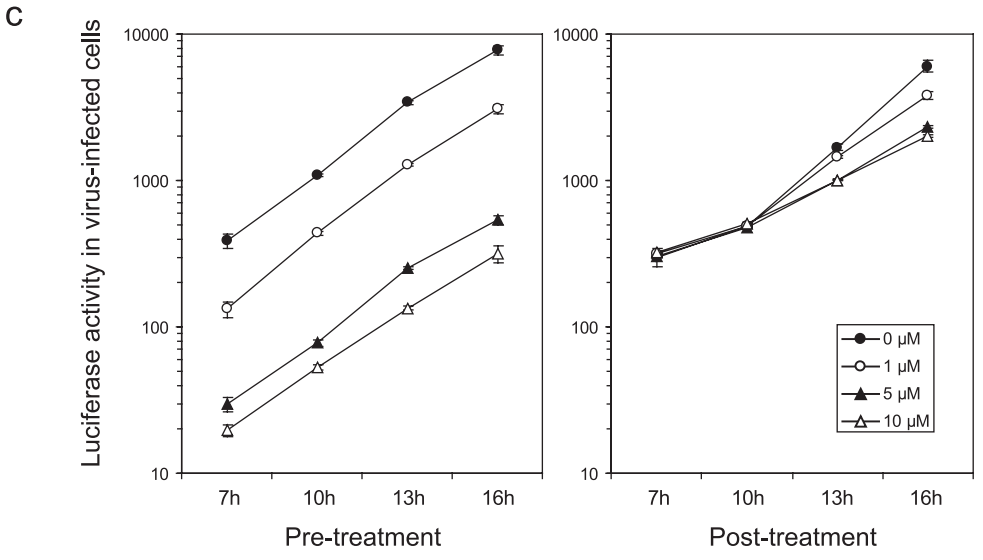

TABLE 1. Summary of the effects of point mutations introduced into two furin sites on S protein cleavage, induction of cell-cell fusion, and recovery of infectious rIBV

S gene mutation site	Name	Prediction of furin cleavage[a]		Cleavage[b]		Cell-cell fusion[c]		Recovery of rIBV[d]
		S1/S2 site (positions 531–539)	2nd site (positions 684–692)	S1/S2	2nd	Try$^-$	Try$^+$	
Wild type	WT	GTRRFR**RS**I	PSSRRR**RS**V	+	+	+++	+++	+
S1/S2	M1	GTAAFAASI	PSSRRR**RS**V	−	+	++	++	+
	Δ1	GT-----SI	PSSRRR**RS**V	−	+	++	++	+
2nd	M2	GTRRFR**RS**I	PSSAAAASV	+	−	−	−	−
	Δ2	GTRRFR**RS**I	PSS----SV	+	−	−	−	−
	M2.1	GTRRFR**RS**I	PSSPRRRSV	+	−	−	++	+
	M2.2	GTRRFR**RS**I	PSSRAAASV	+	−	−	+	−
	M2.3	GTRRFR**RS**I	PSSARAASV	+	−	−	+	−
	M2.4	GTRRFR**RS**I	PSSAARASV	+	−	−	+	−
	M2.5	GTRRFR**RS**I	PSSAAARSV	+	−	+	++	+
Both sites	M1 + 2.1	GTAAFAASI	PSSPRRRSV	−	−	−	++	+
Other	S(Δ538-690)	GTRRFRR--	-------**S**V	+	None	−	−	−

[a] The predicted cleavage position is in boldface.
[b] Cleavage at two furin sites in HuH-7 cells expressing pKT-S(1-789)Fc is indicated by + for yes and − for no cleavage.
[c] Cell-cell fusion at neutral pH in Vero cells expressing pKT-S is indicated by +++ for strong, ++ for mild, + for weak, and − for no induction.
[d] Recovery of infectious rIBV in Vero cells is indicated by + for yes and − for no.

This observation is unique for IBV and differs from MHV A59 and SARS-CoV, whose entry was not inhibited by furin inhibitor (16, 23). Posttreatment of virus-attached cells (4°C) did not block the entry, suggesting that furin may be involved in a step immediately after viral attachment to cells (Fig. 3a, posttreatment at 4 h at 4°C). At 16 h postinfection, the influence of pretreatment on viral infection was more pronounced (Fig. 3a, pretreatment at 16 h), though inhibition of viral replication was also observed in posttreated cells (Fig. 3a, posttreatment at 16 h). There was no significant difference between 5 and 10 μM treatments in this experiment.

The effect of furin inhibitor on syncytium formation was investigated at 16 h postinfection by IF staining. The number of giant syncytia (by primary infection) was significantly decreased in a concentration-dependent manner by pretreatment, but the sizes of these syncytia were not affected (Fig. 3b, pretreatment). The reduction in tiny infected cells (by secondary infection) may have been caused by reduced viral release from the primary infection (Fig. 3b, pretreatment). In contrast, syncytium formation by primary infected cells was blocked by posttreatment in a concentration-dependent manner (Fig. 3b, posttreatment). In addition, the number of smaller syncytia was slightly reduced in posttreated cells (Fig. 3b, posttreatment). The $TCID_{50}$ of viruses released into the culture supernatants and the S protein expression level in virus-infected cells were also investigated at 16 h postinfection. Inhibition of WT infection by furin inhibitor was observed in both experiments (data not shown).

To investigate the kinetics of viral entry and replication in the presence of furin inhibitor, Vero cells were infected with rIBV-Luc. Following infection, the luciferase activity usually started to increase at 6 h and reached the maximum level at 16 h postinfection. As shown in Fig. 3c, analysis of the luciferase activity in virus-infected cells at 7 h postinfection revealed that pretreatment significantly reduced the viral infection in a concentration-dependent manner (Fig. 3c, pretreatment at 7 h), while posttreatment did not show any effect (Fig. 3c, posttreatment at 7 h). These results further confirmed that furin inhibitor blocked viral entry but not replication. Since the degrees of increment of the luciferase activity in pretreated cells were similar regardless of furin inhibitor concentrations (Fig. 3c, pretreatment at 7 to 16 h), less viral replication at higher concentrations of furin inhibitor may be largely due to less primary infection. In posttreated cells, a difference in the luciferase activity was observed from 13 h postinfection in a concentration-dependent manner (Fig. 3c, posttreatment at 13 and 16 h). Since formation of large and tiny syncytia was observed around this time point, less viral replication in posttreated cells was likely due to blocking of cell-to-cell spread and secondary infection.

FIG. 3. Entry and syncytium formation of IBV are blocked by furin inhibitor. (a) Pretreatment with furin inhibitor did not affect attachment but blocked IBV entry. The gRNA level in virus-infected cells was investigated with a quantitative real-time RT-PCR. The values are shown as relative amounts against 0 μM of furin inhibitor treatment. ND, not done. The error bars indicate standard deviations of the means. (b) The number of infected cells was reduced by pretreatment with furin inhibitor, while posttreatment blocked giant syncytium formation. Syncytium formation was observed by IF staining with the S2 Ab at 16 h postinfection. Giant syncytia caused by primary infection are indicated by arrows. (c) Inhibitory effects of pretreatment with furin inhibitor were caused by less primary infection, while those of posttreatment were due to blocking of cell-to-cell spread and secondary infection. The effects of furin inhibitor treatments on rIBV-Luc infection were investigated. Luciferase activity in virus-infected cells was measured at 7, 10, 13, and 16 h postinfection. The error bars indicate standard deviations of the means.

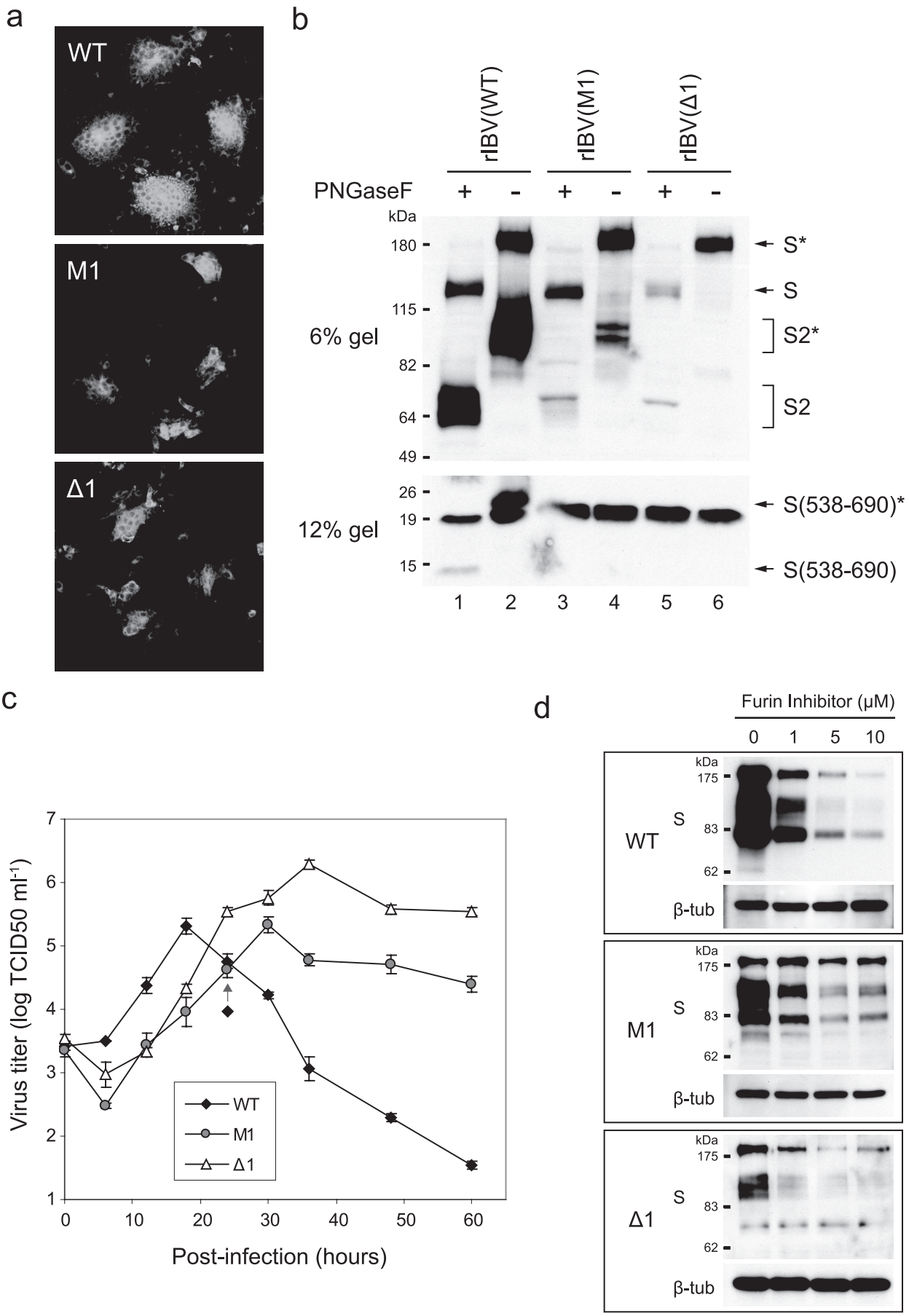

S1/S2 cleavage mediated by furin is not essential for, but could promote, syncytium formation and infectivity of IBV. The contributions of S1/S2 cleavage by furin to IBV infection were investigated by the introduction of mutations into the constructs and the rIBV genome. The four R residues at the S1/S2 cleavage site were removed either by replacement with alanine (A; M1) or by deletion (Δ1) (Table 1), resulting in the ablation of S1/S2 cleavage with no effect on the second-site cleavage (Table 1). Furthermore, the absence of the first furin site (M1 and Δ1) reduced the induction of cell-cell fusion by the S construct (Table 1).

Two mutant viruses, rIBV(M1) and rIBV(Δ1), carrying the mutations/deletion at the S1/S2 site were successfully recovered in Vero cells (Table 1). Consistent with an in vitro cell-cell fusion assay, M1 and Δ1 mutant viruses demonstrated the formation of smaller syncytia than the WT (Fig. 4a). WB results showed that minute amounts of S2* and S2 bands were still detectable in M1- and Δ1-infected cells (Fig. 4b, lanes 3 to 6), demonstrating that the S1/S2 cleavage was not completely eliminated. Once again, multiple S2 bands were detected in WT-infected cells (Fig. 4b, lanes 1 to 6), as observed in cells infected with S-Flag539 and S-Flag1163 viruses (Fig. 2c). These results suggest that inefficient cleavage of IBV S protein in the region flanking the S1/S2 site may also occur at multiple positions, as reported for cleavage of SARS-CoV S protein by trypsin and cathepsin (8). The dual-cleavage fragment [S(538-690)* and S(538-690)] was detected only from cells infected with WT (Fig. 4b, lanes 1 and 2). Analysis of the growth kinetics of the two mutant viruses showed that the replication of M1 and Δ1 was significantly delayed compared to that of the WT, especially at early time points of infection (Fig. 4c). Cytopathic effect (CPE) was usually observed in nearly 100% of cells infected with the WT at 24 h postinfection; the infected cells were rapidly detached and died. In cells infected with M1 and Δ1, about 20% of the cells did not show CPE at 60 h postinfection. Prolonged replication of M1 and Δ1 indicated that cleavage at the S1/S2 site facilitates IBV infection and is important for efficient infection in Vero cells. The effects of pretreatment with furin inhibitor on the infectivity of the two mutant viruses were then tested, showing that, similar to the WT, infection by both M1 and Δ1 was inhibited by furin inhibitor in a concentration-dependent manner (Fig. 4d).

The $XXXR_{690}$/S motif at the second IBV furin site is a minimal sequence to support IBV infection in Vero cells. The four R residues at the second furin site were removed by either R-to-A substitutions or deletion (Table 2, M2 and Δ2). The amino acid sequence of M41 (the parental strain of Beaudette) was also reproduced at the second furin site (M2.1; PRRRS). An additional construct, M1+2.1, was made by combining the mutations of M1 and M2.1 (Table 1). Expression of M2, Δ2, and M2.1 constructs showed cleavage at the S1/S2 site, but not at the second furin site (Table 1). No cleavage at both positions was observed when M1+2.1 was expressed (Table 1). Interestingly, cell-cell fusion at neutral pH was not observed in Vero cells expressing M2, Δ2, M2.1, and M1+2.1 constructs, which lack the second furin site (Table 1). Cell-cell fusion was activated by incubation of cells expressing M2.1 and M1+2.1, but not M2 and Δ2, with 2 μg/ml trypsin for 2 h (Table 1 and Fig. 5a), suggesting that the presence of a trypsin-cleavable motif (R/S) is essential for induction of cell-cell fusion by these mutant constructs. It also indicates that these mutant S proteins could be translocated to the cell surface and that they are functional.

Four additional constructs (M2.2 to M2.5) with monobasic motifs at the second furin site were made by A-to-R substitutions based on mutant construct M2 (Table 1). Sequence analysis with the peptide cutter program (http://www.expasy.ch/tools/peptidecutter/) showed that the probabilities of cleavage by trypsin are 91.9, 100, 100, and 100% for R_{687}AAAS (M2.2), AR_{688}AAS (M2.3), AAR_{689}AS (M2.4), and $AAAR_{690}$S (M2.5), respectively, although they are not cleavable by furin. Neither cleavage at the second furin site nor cell-cell fusion was observed in cells expressing the M2.2 to M2.4 S constructs (Table 1). Interestingly, a single R_{690} residue (M2.5; AAARS) was sufficient to induce weak cell-cell fusion in Vero cells, even though M2.1 with the PRRRS sequence was unable to do so (Table 1). However, it was inefficient compared to the WT, M1, and Δ1, whose second site was a furin consensus motif, RRRR/S. As expected, activation of cell-cell fusion by trypsin was observed in cells expressing constructs bearing a trypsin-cleavable motif (R/A or R/S) at the second site (Table 1 and Fig. 5a). It was also noted that cell-cell fusion was less efficiently induced in cells expressing M2.2 to M2.4 than in those expressing M2.1 and M2.5, probably due to reduced cleavage efficiencies by trypsin at the second site.

These mutations were then introduced into the IBV genome, and infectious viruses were successfully recovered in Vero cells electroporated with M2.1, M1+2.1, and M2.5 constructs, but not with M2, Δ2, M2.2, M2.3, and M2.4 (Table 1), although the 64-terminal-residue sequence which mediates S protein incorporation into the CoV particle (25) is maintained. As no infectious virus was recovered with M2, Δ2, M2.2, M2.3, and M2.4 mutant transcripts, RT-PCR amplification of the negative-strand gRNA and the subgenomic mRNAs was performed at 48 h postelectroporation of transcripts. As shown in Fig. 5b, both negative-strand gRNA and subgenomic mRNAs (mRNA3 and -4) were detected in cells electroporated with these transcripts (lanes 2 and 3). These data indicated that the

FIG. 4. S1/S2 cleavage by furin is not essential for, but could promote, syncytium formation and infectivity of IBV. (a) Cleavage deficiency at the S1/S2 site resulted in reduced size of syncytia. Syncytium formation was observed as described in the legend to Fig. 2a. (b) A minute amount of S1/S2 cleavage was detected in M1- and Δ1-infected cells, although they do not have a furin consensus motif. HuH-7 cells were infected with rIBV for 18 h. Cell extracts (20 μg protein) were analyzed by immunoblotting them with the S2 Ab. (c) Viral replication and spread were reduced in the absence of S1/S2 cleavage. Growth kinetics was investigated as described in the legend to Fig. 2b. The arrow indicates the time point when CPE was observed in nearly 100% of the cells. The error bars indicate standard deviations of the means. (d) Infection of M1 and Δ1 were inhibited by pretreatment with furin inhibitor. Vero cells were pretreated with different concentrations of furin inhibitor and infected with rIBV for 2 h. The cells were washed three times with PBS and incubated with fresh DMEM without furin inhibitor. Replication of viruses was observed by immunoblotting them with the S2 Ab at 16 h postinfection. β-tub, β-tubulin.

TABLE 2. Predicted cleavage by furin, general PCs or trypsin at the XXXR/S motif of CoV S proteins and effects on cleavage and induction of cell-cell fusion by the reproduction of sequence in the second IBV furin site

Group	Species and strain	Summary of cleavage prediction					Reproduction in IBV S			Accession no.
		Position	Sequence[a]	Score and probability[b]			CL[c]	Fusion[d]		
				Furin	PCs	Try (%)		Try$^-$	Try$^+$	
1	Canine	966	NSKRKYR/SA	**0.638**	**0.858**	100	+	++	++	EU856361 and -2
1a	TGEV	956	NSKRKYR/SA	**0.638**	**0.858**	100	+	++	++	NC_002306
	Feline 1683	963	NSKRKYR/SA	**0.638**	**0.858**	100	+	++	++	X80799
	1146, DF-2	961, 963	NSKRKYG SA				−	−	+	NC_007025, DQ286389
	UCD1	969	PPRVGQR/SA	0.148	0.146	100				AB088222
	NTU2, C1Je	979	PPRIGKR/SA	0.314	**0.873**	100				DQ160294, DQ848678
	Black	976	PPKIGVR/SA	0.117	0.146	100				EU186072
1b	Human 229E	689	GSRVAGR/SA	0.212	0.208	100	−	+	++	NC_002645
	NL63	870	SSRIAGR/SA	0.168	0.334	100	−	+	++	NC_005831
	PEDV[e]	891	GRVVQKR/SV	**0.611**	**0.808**	100				NC_003436
	Bat 1A	889	PRQHQSR/SA	0.239	0.112	100				NC_010437
	1B	889	PRQRQSR/SA	**0.592**	**0.513**	100				NC_010436
	512	885	PANPGAR/SV	0.199	0.242	100				NC_009657
	HKU2	671	SERFESR/SV	0.218	0.267	100				NC_009988
	HKU8	894	PQGGGKR/SV	0.307	0.224	100				NC_010438
2	Equine	913	CNTVSSR/SA	0.147	0.199	100				NC_010327
2a	Bovine	913	CNKVSSR/SA	0.178	0.272	100				NC_003045
	Human HKU1	904	HCGSSSR/SF	0.116	0.238	100				NC_006577
	OC43	911	CSKASSR/SA	0.144	0.169	100				NC_005147
	HEV[f]	899	CNRASTR/SA	0.162	0.314	100				NC_007732
	MHV A-59, JHM	869, 921	PSAIRGR/SA	0.188	0.392	100	−	++	++	NC_001846, NC_006852
	BHK	876	PRAIRRR/SA	0.416	**0.586**	89.7				AY497331
	MHV-2	907	MAAQTGR/SA	0.166	0.136	100	−	++	++	AF201929
2b	SARS	797	PLKPTKR/SF	0.261	**0.796**	100	−	−	++	NC_004718
	Bat Rf1	783	PLKPTKR/SF	0.264	**0.796**	100	−	−	++	NC_009695
	HKU3, etc.	783, 784	PSKPTKR/SF	0.296	**0.896**	100				NC_009693, -4, and -6
2c	Bat 133	884	IGGSSYR/SA	0.169	0.226	100				NC_008315
	HKU4-1	886	GSSSSYR/SA	0.264	**0.682**	100				NC_009019
	HKU5-1	884	TGERKYR/ST	**0.507**	**0.681**	100				NC_009020
2d	Bat HKU9-1	809	CGATTYR/SA	0.153	0.123	100				NC_009021
3	IBV M41	690	PSSPRRR/SF	0.304	**0.862**	75.3	−	−	++	AY851295
	WT	690	PSSRRRR/SV	**0.837**	**0.946**	75.3	++	+++	+++	AAY24443
	M2.1	690	PSSPRRR/SV	0.499	**0.937**	75.3	−	−	++	This study
	M2.5	690	PSSAAAR/SV	0.284	0.074	100	−	+	++	This study
	Turkey	704	LAQNQGR/ST	0.140	0.122	100				NC_010800
	Bulbul	677	TSKAGGR/SA	0.147	0.080	100				NC_011548
	Thrush	707	PNKQGGR/SA	0.131	0.067	100				NC_011549
	CoV SW1	973	SDPRDAR/SA	0.382	0.402	100				NC_010646
	Munia	669	SNKIGEK/SV	0.099	0.093	100				NC_011550

[a] The predicted cleavage site by furin, general PCs, or typsin is indicated by a slash.
[b] Scores above 0.5 are in boldface.
[c] Cleavage (CL) at the second furin sites in HuH-7 cells expressing pKT-S(1-789)Fc is indicated by ++ for strong, + for weak, and − for none.
[d] Cell-cell fusion at neutral pH in Vero cells expressing pKT-S is indicated by +++ for similar to WT, ++ for mild, + for weak, and − for none.
[e] PEDV, porcine epidemic diarrhea virus.
[f] HEV, porcine hemagglutinating encephalomyelitis virus.

inability to recover infectious viruses from these constructs was due to S protein modification and that R residues at the second furin site may play a role in the function and conformation of S protein. Therefore, the $XXXR_{690}$/S motif at the second furin site was likely the minimal sequence required to support IBV infectivity in Vero cells.

An additional construct, S(Δ538-690), with deletion of the region between the two furin sites, was also made; however, no induction of cell-cell fusion and recovery of the infectious virus was observed (Fig. 5a and Table 1). Amplification by RT-PCR detected both negative-strand gRNA and subgenomic RNAs in Vero cells electroporated with S(Δ538-690) transcripts (Fig. 5b, lane 8), confirming that the mutation did not affect the replication and transcription of viral RNA.

Proteolytic activation at the second IBV furin site is mediated by furin and other serine protease(s). The recovered

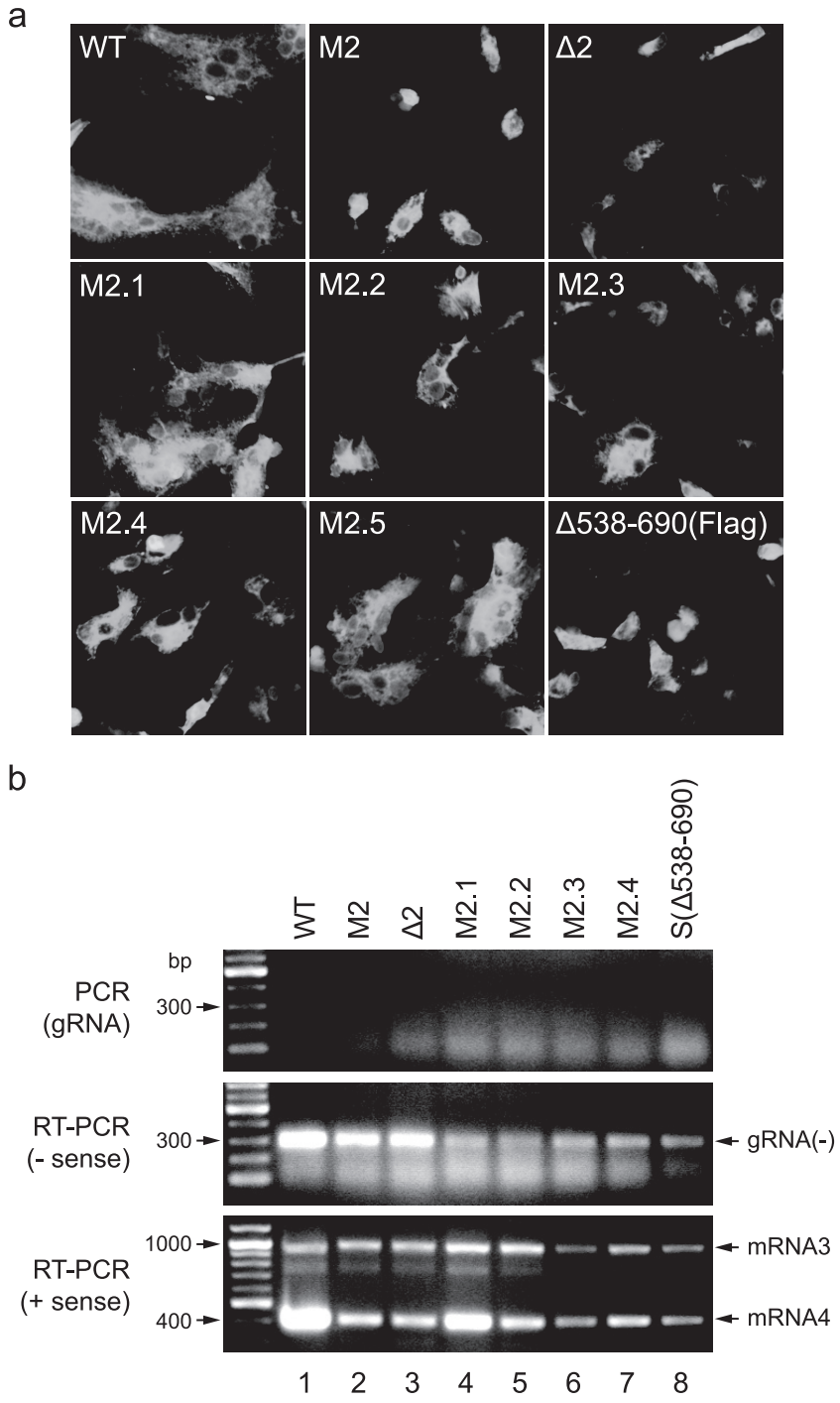

FIG. 5. Infectivity to Vero cells was abrogated by mutations of the second furin site in S protein. (a) Trypsin activation of cell-cell fusion was inefficient in the second furin site mutants, which cannot recover infectious viruses. Trypsin (2 μg/ml) was added at 10 h posttransfection of S constructs, and the cells were incubated for 2 h at 37°C. IF staining was carried out with either anti-S2 or anti-Flag Ab. (b) Replication and transcription of viral RNAs were observed in cells electroporated with mutant transcripts, although the infectious clones were not recovered. At 48 h postelectroporation of the full-length transcripts, total RNA was extracted from the cells. Negative-strand gRNA and subgenomic mRNA were detected by RT-PCR amplification.

mutant viruses M2.1, M1+2.1, and M2.5 were then characterized. M2.1 and M1+2.1 did not induce syncytium formation in Vero cells (Fig. 6a). Instead, rounded single cells were noticed from 24 h postinfection in M2.1- and M1+2.1-infected cells (Fig. 6a) (only M2.1 is shown). Delayed syncytium formation was observed in M2.5-infected cells compared to the WT, M1, and Δ1 viruses (Fig. 6a). The smaller syncytia induced by M2.5 were usually seen only at 24 to 30 h postinfection in Vero cells.

WB results confirmed that cleavage at the S1/S2 site occurred efficiently in M2.1 and M2.5 but not in M1+2.1 (Fig.

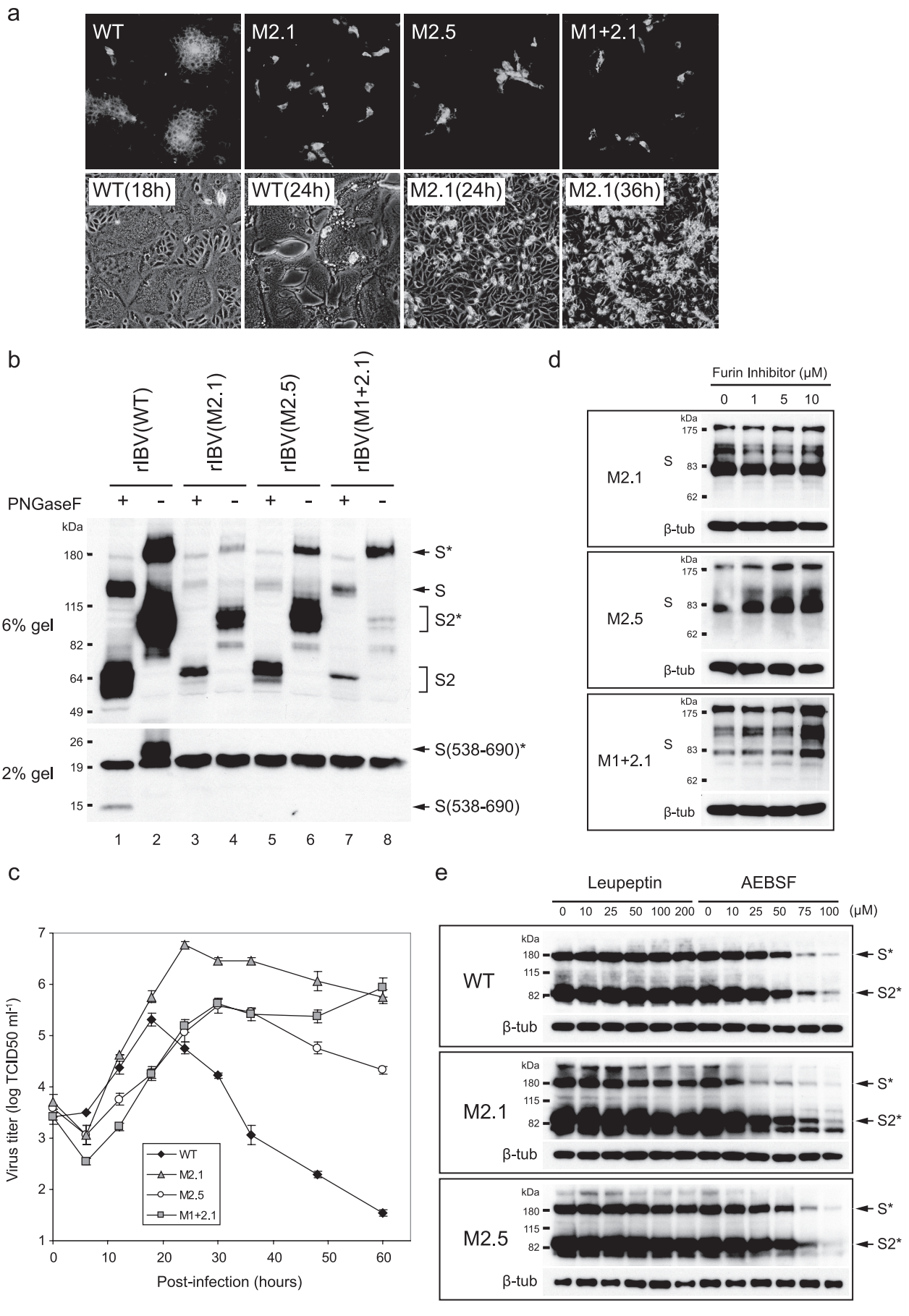

6b). The dual-cleavage fragment [S(538-690)* and S(538-690)] was detected only in cells infected with WT (Fig. 6b). Analysis of the growth kinetics showed that the replication of all mutant viruses was delayed, reaching peak titer at 24, 30, and 60 h postinfection for M2.1, M2.5, and M1+2.1, respectively (Fig. 6c). Interestingly, both M2.1 and M1+2.1 mutant viruses produced higher titers, with M2.1 reaching a peak titer of nearly 10^7, more than 1 log unit higher than the WT (Fig. 6c). Without formation of syncytia, rounded cells remained scattered at 60 h postinfection, with prolonged replication and production of high titers of virus (Fig. 6c). The much delayed replication of M1+2.1 compared to M2.1 further supported the conclusion that S1/S2 cleavage by furin facilitates infection by IBV in Vero cells. The growth kinetics of M2.5 that induces syncytium formation was similar to that of M1 virus (Fig. 6c, M2.5, and 4c, M1).

Pretreatment of M2.1, M2.5, and M1+2.1 with furin inhibitor showed that infection by the three mutant viruses was not inhibited, suggesting that furin dependence of IBV entry was mediated by the second furin site (Fig. 6d). Taken together, the evidence shows that proteolytic activation of IBV S protein by furin occurs at the second furin site for both virus-cell and cell-cell fusion events, but not S1/S2 cleavage.

To test whether proteolytic activation of M2.1 and M2.5 S proteins is mediated by a trypsin-like protease(s), the effects of two broad-range protease inhibitors, leupeptin (a cysteine and serine protease inhibitor) and AEBSF (a serine protease inhibitor), at concentrations from 0 to 200 μM were investigated. In the presence of AEBSF, but not leupeptin, inhibition of WT infection was observed in a concentration-dependent manner (Fig. 6e), consistent with the inhibitory effects of those agents on furin activity. Pretreatment with leupeptin did not inhibit either M2.1 or M2.5 infection (Fig. 6e). In contrast, treatment with AEBSF reduced infection by M2.1 and M2.5 in a concentration-dependent manner (Fig. 6e). These data demonstrate that the entry of M2.1 and M2.5 is also mediated by a yet-to-be-identified serine protease(s). As the infectivity of M2.1 and M2.5 mutant viruses was not inhibited by leupeptin, this rules out the possibility that the mutant S proteins may be activated in Vero cells by type II transmembrane serine proteases, which cleave monobasic motifs, as shown with influenza A virus hemagglutinin (10, 11, 28). Differences in the infectivity and syncytium formation of these mutant viruses may be due to the expression level and cellular localization of the associated protease(s) and the cleavage efficiency of the substrate sequence.

The minimal XXXR/S motif, cleavable by furin, general PCs, or trypsin, is strictly conserved at the equivalent position of the second IBV furin site in most CoV S proteins. As demonstrated above, $XXXR_{690}$/S is likely the minimal motif of IBV S protein at the second furin site, and the associated proteases may vary depending on the first 3 amino acids. Analysis of 52 published IBV S protein sequences by multiple alignments, the ProP server, and the peptide cutter program showed that only the Beaudette-related strains (15/52) are cleavable by furin at the second furin site. However, most S proteins (36/52) could be cleaved by general PCs, including PC1, PC2, furin, PC4, PC5, PACE4, and PC7, and all (52/52) by trypsin at this position, confirming that the XXXR/S motif is strictly conserved. The same analysis also showed that all S proteins (52/52) are furin cleavable at the S1/S2 site.

Similar analysis was then extended to other CoVs. As expected, similarity analysis of CoV S proteins showed that the S2 domain, but not the S1 domain, is conserved (Fig. 7). The low similarity (gaps) in the S1 domain was largely due to amino acid insertions in group 1 (at positions 1 to 200) and group 2 (at 730 to 880) (Fig. 7). The S1/S2 cleavage site was mapped to the variable region, and the second IBV furin site straddled the variable and consensus regions (Fig. 7). The multiple alignments and furin site prediction showed the presence of a furin site at a position equivalent to the second IBV furin site in group 1 CoVs, including canine CoV, FECV 1683, porcine epidemic diarrhea virus, transmissible gastroenteritis virus (TGEV), and bat CoV 1B, and group 2 bat CoV HKU5-1 (Table 2). However, the low probability score and the lack of a preferred motif, RXR(K)R, indicate that cleavage may be inefficient. Analysis of the predicted cleavage by general PCs showed the presence of a cleavable site in feline CoV (NTU2 and C1Je), group 2 CoVs (MHV BHK, SARS-CoV, and bat CoV), and IBV M41 (Table 2). The minimal XXXR/S motif is strictly conserved in most examined CoVs, with the exception of FIPV strains 1146 and DF-2, in which the R residue was replaced by a G (NSKRKY$G_{961\ or\ 963}$S) (Table 2). The equivalent positions in other feline CoV S proteins are an XXXR/S motif and a furin site (underlined) (NSK<u>RKYR</u>$_{963}$/S), found in FECV 1683, as well as canine CoV and TGEV (Table 2). Cathepsin B, but not cathepsin L, was shown to mediate cleavage of the FIPV 1146 S protein at a position further downstream from the S1/S2 cleavage site (43). Cleavage of the FECV 1683 S protein occurs at the same position but is mediated by both cathepsins B and L (43). The S protein of munia CoV has an R-to-K substitution (underlined) (SNKIGE<u>K</u>$_{669}$/SV), which is cleavable by trypsin (Table 2).

Replacement of the second IBV furin site with FIPV 1146 (NSKRKYGS) and FECV 1683 (NSKRKYR/S) sequences showed induction of mild cell-cell fusion in Vero cells expressing the FECV sequence, but not the FIPV sequence (Table 2).

FIG. 6. Proteolytic activation at the second IBV furin site is mediated by furin and other serine protease(s). (a) Giant syncytium formation by rIBV was mediated by proteolytic activation at the second furin site. Syncytium formation was observed as described in the legend to Fig. 2a. For observation of CPE, cells were incubated with DMEM instead of overlay medium. (b) S1/S2 cleavage occurred efficiently in M2.1- and M2.5-infected cells, but not in M1+2.1-infected cells. HuH-7 cells were infected with rIBV for 18 h. Cell extracts (20 μg protein) were analyzed by immunoblotting them with the S2 Ab. (c) M2.1 and M1+2.1, which lack induction of syncytia, demonstrated prolonged replication with high productivity of virions. The growth kinetics was investigated as described in the legend to Fig. 2b. The error bars indicate standard deviations of the means. (d) Infection of M2.1, M1+2.1, and M2.5 was not affected by pretreatment with furin inhibitor. The effect of pretreatment with furin inhibitor was investigated as described in the legend to Fig. 4d. (e) Infection of the WT, M2.1, and M2.5 was inhibited by pretreatment with AEBSF, but not leupeptin. The effects of protease inhibitors were investigated as described in the legend to Fig. 4d, except that the cells were pretreated with leupeptin or AEBSF.

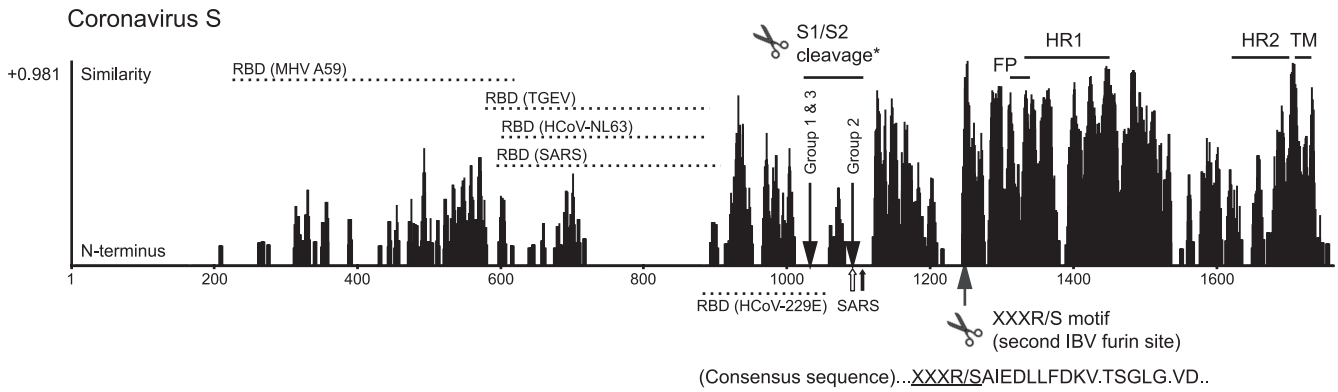

FIG. 7. A novel XXXR/S motif, cleavable by furin, general PCs, or trypsin, is strictly conserved in CoV. The similarity alignments of CoV S were obtained with the Vector NTI Align X software (Informax). The fusion peptide (FP), heptad repeats 1 and 2 (HR1 and HR2), and the transmembrane domain (TM) are also shown. The gaps in the HR1 and HR2 regions were due to amino acid insertion in a group 1 CoV. Receptor-binding domains (RBD) are shown with dashed lines. The S1/S2 cleavage and the second IBV furin site are indicated by arrows. The asterisk indicates the site of S1/S2 cleavage by furin in group 1 (feline CoV Black and NTU2), group 2 (MHV, bovine CoV, human CoV OC43 and HKU-1, porcine hemagglutinating encephalomyelitis virus, and equine CoV), and group 3 (IBV and turkey CoV). S1/S2 cleavage in SARS-CoV by trypsin (empty arrow) and cathepsin (solid arrow) is also shown.

However, cell-cell fusion could be activated upon trypsin treatment in cells expressing the FIPV sequence, suggesting that the FIPV sequence is trypsin cleavable at the NSKRKYGS position (underlined). The probabilities of cleavage by trypsin were 65, 89.7, and 84.3% for $NSK_{957}R_{958}K_{959}YGS$ at positions $K_{957,}$ R_{958}, and K_{959}, respectively. Furthermore, cleavage by furin at the second site was detectable in cells expressing the chimeric S(1-789) construct containing the FECV, but not FIPV, sequence (Table 2), suggesting that the RKYR/S motif in FECV, TGEV, canine CoV, and bat CoV HKU5-1 is furin cleavable. These data indicated that the RXXR motif is a minimal furin-cleavable sequence, as in the hepatitis B virus e antigen (30).

Similarly, replacement of the second IBV furin site with the equivalent sequences from human CoV 229E (GSRVAGR/S) and NL63 (SSRIAGR/S), MHV (PSAIRGR/S), MHV-2 (MA AQTGR/S), and SARS-CoV (PLKPTKR/S) showed induction of either mild or weak cell-cell fusion in cells expressing MHV, MHV-2, human CoV 229E, and human CoV NL63, but not SARS-CoV, sequences (Table 2). It suggests that induction of cell-cell fusion by these S constructs may be activated by a yet-to-be-identified trypsin-like protease(s), as in M2.5. Upon trypsin treatment, more extensive cell-cell fusion was observed in cells expressing the SARS-CoV sequence (Table 2) than in cells expressing the FIPV sequence, suggesting that $XXXR_{690}S$ may be a preferred motif in the context of the IBV S protein. Nevertheless, these results confirm that the equivalent motifs in other CoV S proteins can be efficiently activated by trypisn-like proteases in the context of the IBV S protein.

DISCUSSION

To date, two different pathways have been reported for CoV entry. The entry of feline CoV, human CoV 229E, IBV (M41 and egg-adapted Beaudette), MHV A59, MHV-2, and SARS-CoV takes place via the endosomal pathway (14, 20, 31, 41, 43, 45), while MHV JHM enters cells directly from the plasma membrane (24). However, this process is known to be species- or strain-specific in CoV, due to differences in the receptor-binding regions of individual S proteins (4, 26, 36, 37, 47), in pH dependence in inducing conformational change of the S protein (35, 54), and especially in the cleavability of S proteins (3, 15, 16, 29, 43). It would be crucial to understand how proteolytic activation of CoV S protein occurs, since it is far from the typical type I viral fusion protein, in which furin cleavage exposes the fusion peptide. In this study, we identified a furin activation site implicated in the entry and syncytium formation of Vero-adapted IBV. It is located 153 amino acids downstream of the first furin site (the S1/S2 cleavage site), and the amino acid sequence of the cleavage site determines the serine proteases for S protein activation.

Our findings are likely applicable to other CoVs, since the XXXR/S motif is strictly conserved. Replacement of the second IBV furin site with other CoV sequences demonstrated that the motif is functional in the context of IBV S protein. Furthermore, SARS-CoV acquired the cathepsin L-independent cell surface pathway for entry by mutation of the equivalent motif from $PTKR_{801}/S$ (R_{797} in NC_004718) to furin-cleavable $RRKR_{801}/S$ (cl-S) (50), indicating that protease associated with the entry of SARS-CoV(cl-S) was switched from cathepsin L to, most likely, furin. In addition, SARS-CoV(cl-S) induced cell-cell fusion at neutral pH (50), suggesting that proteolytic activation is a common mechanism for induction of virus-cell and cell-cell fusion, as observed in IBV, and that cell-cell fusion is dependent on the cell surface expression of proteases. Taking the data together, a novel XXXR/S motif at the S2 domain is likely a common site for proteolytic activation in CoV S protein. The first 3 amino acids (underlined) (XXXR/S) of the site are located in the variable region of the S2 domain, and the last 2 amino acids (XXXR/S) are located in the consensus region. The diversity of proteases associated with proteolytic activation, therefore, may be explained by different amino acid sequences at the site. The proteolytic activation process of CoV S protein exposes a highly conserved motif, SAIEDLLFDKV, at the N terminus of the fusion protein. The involvement of this consensus domain in membrane fusion events would also be an interesting topic for further studies.

Inhibition of CoV infection by furin inhibitor was previously reported for MHV A59 and SARS-CoV (16, 23). In both cases, furin inhibitor blocks cell-cell fusion but does not affect entry. It was speculated that requirements for virus-cell and cell-cell fusion could be different in CoV membrane fusion. However, the trigger for both membrane fusion events by IBV Beaudette S protein was shown to be furin activation at the second site. The amino acid sequences at the equivalent position in MHV A59 and SARS-CoV are IRGRS and PTKRS, respectively, with no other potential furin sites found nearby. The inhibitory effect of furin inhibitor, therefore, may be limited to S1/S2 cleavage, which promotes cell-cell fusion, as observed in this study. The observation that entry of M2.1 and M2.5 mutant viruses was not influenced by pretreatment with furin inhibitor may explain why furin inhibitor blocks cell-cell fusion but does not affect the entry of MHV A59 and SARS-CoV.

Cleavage of IBV S protein may preferentially occur at the S1/S2 site, as a putative N-terminal cleavage intermediate up to the second site was not detected in the infected cells, although S1, S2, and the dual-cleavage product were usually detected. The IBV S1/S2 site is likely to be an ideal furin substrate, as full cleavage at this position could be detected, especially in chicken embryos (13). Cleavage of the MHV S protein at this position may take place during its transport to the plasma membrane, but the efficiency varies based on the amino acid sequences of different MHV S proteins at the site (5). Preferential cleavage of the SARS-CoV S protein may also occur at the S1/S2 cleavage site in the presence of a low concentration of trypsin, while cleavage at other positions requires higher concentrations of trypsin (35). The requirement for furin in IBV entry suggests that cleavage at the second site may occur in the supernatant or upon attachment of the virus to a functional receptor. Binding to the receptor may in turn trigger a conformational change of S protein coupled with cleavage at the S1/S2 site by furin or alternative proteases, unmasking the second furin site. This may explain why S1/S2 cleavage by furin enhances IBV infection, even though the entry of IBV is likely triggered by furin activation at the second site. Cleavage at the second site may take place immediately upon viral attachment, since posttreatment of virus-attached cells with furin inhibitor did not block entry. As in SARS-CoV(cl-S) (50), the entry of Vero-adapted IBV may occur at either the cell surface or the early endosome, as determined by the cellular distribution of furin (9, 39).

The presence of two furin sites was reported in the F proteins of human and bovine RSV (HRSV and BRSV) (55). The 27-amino-acid peptide released by dual cleavage of F protein from BRSV, but not from HRSV, was further subjected to posttranslational modification and converted into virokinin, which is homologous to a family of bioactive peptides, tachykinin (56). Virokinin may play a role in eosinophil recruitment and in induction of pulmonary inflammation (48). The dual-cleavage product of BRSV was also shown to be nonessential, but its amino acid sequence affects the intracellular transport and maturation of F protein, viral entry into target cells, direct spread from cell to cell, and growth (34, 48). Therefore, it may determine the accessibility of the two furin sites of F protein. As in HRSV, the released S(538-690) fragment from IBV S protein does not contain a tachykinin motif. In addition, furin-dependent release is limited to the Beaudette-related strains of IBV, which are attenuated in adult birds, suggesting that the S(538-690) fragment is not associated with IBV pathogenesis. However, as this dual-cleavage fragment is 153 amino acids in length, it may have a more pronounced effect on the conformation of IBV S protein. In fact, deletion of the region [S(Δ538-690)] affected cell-cell fusion and recovery of the infectious viruses.

As in many other enveloped viruses, the cell tropism of IBV is determined by S protein (12). In this study, we have shown that the extended cell tropism of Vero-adapted IBV is not determined by acquisition of the second furin site, since the M1+2.1 mutant virus without both furin sites propagates well in Vero cells. In addition to being the substrate for furin cleavage, the two furin sites could function as HS-binding motifs. The possibility that IBV may utilize cell surface HS as an entry factor during adaptation to cultured cells is ruled out by the observation that pretreatment of Vero cells with heparinase I promoted IBV infection (unpublished data). Furthermore, we previously reported that the S gene cloned from egg-adapted IBV(EP3) contains the second furin site (22); however, infectious rIBV(EP3) could not be recovered (unpublished data). The S protein of Vero-adapted IBV contains multiple mutations in regions immediately downstream of the second furin site, the predicted fusion peptide, HR1, and HR1-2 linker compared to the egg-adapted IBV. These mutations may influence the biochemical properties and function of S protein, as well as the conformation of S protein for virus-cell and cell-cell fusion. Further studies are required to understand the mechanisms underlying the extended cell tropism of Vero-adapted IBV.

ACKNOWLEDGMENTS

This work was supported by the Agency for Science, Technology and Research, Singapore, and a grant from the Biomedical Research Council (BMRC 03/1/22/17/220), Agency for Science, Technology and Research, Singapore.

REFERENCES

1. **Alonso-Caplen, F. V., Y. Matsuoka, G. E. Wilcox, and R. W. Compans.** 1984. Replication and morphogenesis of avian coronavirus in Vero cells and their inhibition by momensin. Virus Res. **1:**153–167.
2. **Basak, A., M. Zhong, J. S. Munzer, M. Chretien, and N. G. Seidah.** 2001. Implication of the proprotein convertases furin, PC5 and PC7 in the cleavage of surface glycoproteins of Hong Kong, Ebola and respiratory syncytial viruses: a comparative analysis with fluorogenic peptides. Biochem. J. **353:**537–545.
3. **Bergeron, E., M. J. Vincent, L. Wickham, J. Hamelin, A. Basak, S. T. Nichol, M. Chretien, and N. G. Seidah.** 2005. Implication of proprotein convertases in the processing and spread of severe acute respiratory syndrome coronavirus. Biochem. Biophys. Res. Commun. **326:**554–563.
4. **Bonavia, A., B. D. Zelus, D. E. Wentworth, P. J. Talbot, and K. V. Holmes.** 2003. Identification of a receptor-binding domain of the spike glycoprotein of human coronavirus HCoV-229E. J. Virol. **77:**2530–2538.
5. **Bos, E. C., L. Heijnen, W. Luytjes, and W. J. Spaan.** 1995. Mutational analysis of the murine coronavirus spike protein: effect on cell-to-cell fusion. Virology **214:**453–463.
6. **Bosch, B. J., B. E. Martina, R. van der Zee, J. Lepault, B. J. Haijema, C. Versluis, A. J. Heck, R. De Groot, A. D. Osterhaus, and P. J. Rottier.** 2004. Severe acute respiratory syndrome coronavirus (SARS-CoV) infection inhibition using spike protein heptad repeat-derived peptides. Proc. Natl. Acad. Sci. USA **101:**8455–8460.
7. **Bosch, B. J., R. van der Zee, C. A. M. de Haan, and P. J. M. Rottier.** 2003. The coronavirus spike protein is a class I virus fusion protein: structural and functional characterization of the fusion core complex. J. Virol. **77:**8801–8811.
8. **Bosch, B. J., W. Bartelink, and P. J. Rottier.** 2008. Cathepsin L functionally cleaves the SARS-CoV class I fusion protein upstream of rather than adjacent to the fusion peptide. J. Virol. **82:**8887–8890.
9. **Bosshart, H., J. Humphrey, E. Deignan, J. Davidson, J. Drazba, L. Yuan, V. Oorschot, P. J. Peters, and J. S. Bonifacino.** 1994. The cytoplasmic domain

mediates localization of furin to the trans-Golgi network en route to the endosomal/lysosomal system. J. Cell Biol. **126:**1157–1172.
10. **Böttcher, E., T. Matrosovich, M. Beyerle, H. D. Klenk, W. Garten, and M. Matrosovich.** 2006. Proteolytic activation of influenza viruses by serine proteases TMPRSS2 and HAT from human airway epithelium. J. Virol. **80:** 9896–9898.
11. **Chaipan, C., D. Kobasa, S. Bertram, I. Glowacka, I. Steffen, T. S. Tsegaye, M. Takeda, T. H. Bugge, S. Kim, Y. Park, A. Marzi, and S. Pöhlmann.** 2009. Proteolytic activation of the 1918 influenza virus hemagglutinin. J. Virol. **83:**3200–3211.
12. **Casais, R., B. Dove, D. Cavanagh, and P. Britton.** 2003. Recombinant avian infectious bronchitis virus expressing a heterologous spike gene demonstrates that the spike protein is a determinant of cell tropism. J. Virol. **77:**9084–9089.
13. **Cavanagh, D., P. J. Davis, D. J. C. Pappin, M. M. Binns, M. E. G. Boursnell, and T. D. K. Brown.** 1986. Coronavirus IBV: partial amino terminal sequencing of spike polypeptide S2 identifies the sequence Arg-Arg-Phe-Arg-Arg at the cleavage site of the spike precursor propolypeptide of IBV strains Beaudette and M41. Virus Res. **4:**133–143.
14. **Chu, V. C., L. J. McElroy, V. Chu, B. E. Bauman, and G. R. Whittaker.** 2006. The avian coronavirus infectious bronchitis virus undergoes direct low-pH-dependent fusion activation during entry into host cells. J. Virol. **80:**3180–3188.
15. **de Haan, C. A., B. J. Haijema, P. Schellen, P. W. Schreur, E. te Lintelo, H. Vennema, and P. J. Rottier.** 2008. Cleavage of group 1 coronavirus spike proteins: how furin cleavage is traded off against heparan sulfate binding upon cell culture adaptation. J. Virol. **82:**6078–6083.
16. **de Haan, C. A., K. Stadler, G.-J. Godeke, B. J. Bosch, and P. J. Rottier.** 2004. Cleavage inhibition of the murine coronavirus spike protein by a furin-like enzyme affects cell-cell but not virus-cell fusion. J. Virol. **78:**6048–6054.
17. **de Haan, C. A., Z. Li, E. te Lintelo, B. J. Bosch, B. J. Haijema, and P. J. Rottier.** 2005. Murine coronavirus with an extended host range uses heparan sulfate as an entry receptor. J. Virol. **79:**14451–14456.
18. **Du, L., R. Y. Kao, Y. Zhou, Y. He, G. Zhao, C. Wong, S. Jiang, K. Y. Yuen, D. Y. Jin, and B. J. Zheng.** 2007. Cleavage of spike protein of SARS coronavirus by protease factor Xa is associated with viral infectivity. Biochem. Biophys. Res. Commun. **359:**174–179.
19. **Duckert, P., S. Brunak, and N. Blom.** 2004. Prediction of proprotein convertase cleavage sites. Protein Eng. Des. Sel. **17:**107–112.
20. **Eifart, P., K. Ludwig, C. Böttcher, C. A. de Haan, P. J. Rottier, T. Korte, and A. Herrmann.** 2007. Role of endocytosis and low pH in murine hepatitis virus strain A59 cell entry. J. Virol. **81:**10758–10768.
21. **Fang, S. G., B. Chen, F. P. Tay, B. S. Ng, and D. X. Liu.** 2007. An arginine-to-proline mutation in a domain with undefined functions within the helicase protein (Nsp13) is lethal to the coronavirus infectious bronchitis virus in cultured cells. Virology **358:**136–147.
22. **Fang, S. G., S. Shen, F. P. Tay, and D. X. Liu.** 2005. Selection of and recombination between minor variants lead to the adaptation of an avian coronavirus to primate cells. Biochem. Biophys. Res. Commun. **336:**417–423.
23. **Follis, K. E., J. York, and J. H. Nunberg.** 2006. Furin cleavage of the SARS coronavirus spike glycoprotein enhances cell-cell fusion but does not affect virion entry. Virology **350:**358–369.
24. **Gallagher, T. M., C. Escarmis, and M. J. Buchmeier.** 1991. Alteration of the pH dependence of coronavirus-induced cell fusion: effect of mutations in the spike glycoprotein. J. Virol. **65:**1916–1928.
25. **Godeke, G. J., C. A. de Haan, J. W. Rossen, H. Vennema, and P. J. Rottier.** 2000. Assembly of spikes into coronavirus particles is mediated by the carboxy-terminal domain of the spike protein. J. Virol. **74:**1566–1571.
26. **Godet, M., J. Grosclaude, B. Delmas, and H. Laude.** 1994. Major receptor-binding and neutralization determinants are located within the same domain of the transmissible gastroenteritis virus (coronavirus) spike protein. J. Virol. **68:**8008–8016.
27. **Hallenberger, S., M. Moulard, M. Sordel, H. D. Klenk, and W. Garten.** 1997. The role of eukaryotic subtilisin-like endoproteases for the activation of human immunodeficiency virus glycoproteins in natural host cells. J. Virol. **71:**1036–1045.
28. **Hooper, J. D., J. A. Clements, J. P. Quigley, and T. M. Antalis.** 2001. Type II transmembrane serine proteases. Insights into an emerging class of cell surface proteolytic enzymes. J. Biol. Chem. **276:**857–860.
29. **Huang, I. C., B. J. Bosch, F. Li, W. Li, K. H. Lee, S. Ghiran, N. Vasilieva, T. S. Dermody, S. C. Harrison, P. R. Dormitzer, M. Farzan, P. J. Rottier, and H. Choe.** 2006. SARS coronavirus, but not human coronavirus NL63, utilizes cathepsin L to infect ACE2-expressing cells. J. Biol. Chem. **281:**3198–3203.
30. **Ito, K., K. H. Kim, A. S. Lok, and S. Tong.** 2009. Characterization of genotype-specific carboxyl-terminal cleavage sites of hepatitis B virus e antigen precursor and identification of furin as the candidate enzyme. J. Virol. **83:**3507–3517.
31. **Kawase, M., K. Shirato, S. Matsuyama, and F. Taguchi.** 2009. Protease-mediated entry via the endosome of human coronavirus 229E. J. Virol. **83:**712–721.
32. **Keelapang, P., R. Sriburi, S. Supasa, N. Panyadee, A. Songjaeng, A. Jairungsri, C. Puttikhunt, W. Kasinrerk, P. Malasit, and N. Sittisombut.** 2004. Alterations of pr-M cleavage and virus export in pr-M junction chimeric dengue viruses. J. Virol. **78:**2367–2381.
33. **Klenk, H. D., and W. Garten.** 1994. Host cell proteases controlling virus pathogenicity. Trends Microbiol. **2:**39–43.
34. **König, P., K. Giesow, K. Schuldt, U. J. Buchholz, and G. M. Keil.** 2004. A novel protein expression strategy using recombinant bovine respiratory syncytial virus (BRSV): modifications of the peptide sequence between the two furin cleavage sites of the BRSV fusion protein yield secreted proteins, but affect processing and function of the BRSV fusion protein. J. Gen. Virol. **85:**1815–1824.
35. **Li, F., M. Berardi, W. Li, M. Farzan, P. R. Dormitzer, and S. C. Harrison.** 2006. Conformational states of the severe acute respiratory syndrome coronavirus spike protein ectodomain. J. Virol. **80:**6794–6800.
36. **Li, F., W. Li, M. Farzan, and S. C. Harrison.** 2005. Structure of SARS coronavirus spike receptor-binding domain complexed with receptor. Science **309:**1864–1868.
37. **Lin, H. X., Y. Feng, G. Wong, L. Wang, B. Li, X. Zhao, Y. Li, F. Smaill, and C. Zhang.** 2008. Identification of residues in the receptor-binding domain (RBD) of the spike protein of human coronavirus NL63 that are critical for the RBD-ACE2 receptor interaction. J. Gen. Virol. **89:**1015–1024.
38. **Liu, D. X., I. Brierley, K. W. Tibbles, and T. D. K. Brown.** 1994. A 100K polypeptide encoded by open reading frame (ORF) 1b of the coronavirus infectious bronchitis virus is processed by ORF1a products. J. Virol. **68:** 5772–5780.
39. **Molloy, S. S., L. Thomas, J. K. VanSlyke, P. E. Stenberg, and G. Thomas.** 1994. Intracellular trafficking and activation of the furin proprotein convertase: localization to the TGN and recycling from the cell surface. EMBO J. **13:**18–33.
40. **Otsuki, K., K. Noro, H. Yamamoto, and M. Tsubokura.** 1979. Studies on avian infectious bronchitis virus (IBV). II. Propagation of IBV in several cultured cells. Arch. Virol. **60:**115–122.
41. **Qiu, Z., S. T. Hingley, G. Simmons, C. Yu, L. Das Sarma, P. Bates, and S. R. Weiss.** 2006. Endosomal proteolysis by cathepsins is necessary for murine coronavirus mouse hepatitis virus type 2 spike-mediated entry. J. Virol. **80:**5768–5776.
42. **Reed, L. J., and H. Muench.** 1938. A simple method of estimating fifty per cent endpoints. Am. J. Hyg. **27:**493–497.
43. **Regan, A. D., R. Shraybman, R. D. Cohen, and G. R. Whittaker.** 2008. Differential role for low pH and cathepsin-mediated cleavage of the viral spike protein during entry of serotype II feline coronaviruses. Vet. Microbiol. **132:**235–248.
44. **Shen, H., S. G. Fang, B. Chen, G. Chen, F. P. Tay, and D. X. Liu.** 2009. Towards construction of viral vectors based on avian coronavirus infectious bronchitis virus for gene delivery and vaccine development. J. Virol. Methods doi:10.1016./j.jviromet/2009.04.023.
45. **Simmons, G., D. N. Gosalia, A. J. Rennekamp, J. D. Reeves, S. L. Diamond, and P. Bates.** 2005. Inhibitors of cathepsin L prevent severe acute respiratory syndrome coronavirus entry. Proc. Natl. Acad. Sci. USA **102:**11876–11881.
46. **Thomas, G.** 2002. Furin at the cutting edge: from protein traffic to embryogenesis and disease. Nat. Rev. Mol. Cell Biol. **3:**753–766.
47. **Tsai, J. C., B. D. Zelus, K. V. Holmes, and S. R. Weiss.** 2003. The N-terminal domain of the murine coronavirus spike glycoprotein determines the CEACAM1 receptor specificity of the virus strain. J. Virol. **77:**841–850.
48. **Valarcher, J. F., J. Furze, S. G. Wyld, R. Cook, G. Zimmer, G. Herrler, and G. Taylor.** 2006. Bovine respiratory syncytial virus lacking the virokinin or with a mutation in furin cleavage site RA(R/K)R109 induces less pulmonary inflammation without impeding the induction of protective immunity in calves. J. Gen. Virol. **87:**1659–1667.
49. **Vidricaire, G., J. B. Denault, and R. Leduc.** 1993. Characterization of a secreted form of human furin endoprotease. Biochem. Biophys. Res. Commun. **195:**1011–1018.
50. **Watanabe, R., S. Matsuyama, K. Shirato, M. Maejima, S. Fukushi, S. Morikawa, and F. Taguchi.** 2008. Entry from the cell surface of severe acute respiratory syndrome coronavirus with cleaved S protein as revealed by pseudotype virus bearing cleaved S protein. J. Virol. **82:**11985–11991.
51. **Winter, C., C. Schwegmann-Wessels, D. Cavanagh, U. Neumann, and G. Herrler.** 2006. Sialic acid is a receptor determinant for infection of cells by avian infectious bronchitis virus. J. Gen. Virol. **87:**1209–1216.
52. **Winter, C., G. Herrler, and U. Neumann.** 2008. Infection of the tracheal epithelium by infectious bronchitis virus is sialic acid dependent. Microbes Infect. **10:**367–373.
53. **Xiao, H., L. H. Xu, Y. Yamada, and D. X. Liu.** 2008. Coronavirus spike protein inhibits host cell translation by interaction with eIF3f. PLoS ONE **3:**e1494.
54. **Zelus, B. D., J. H. Schickli, D. M. Blau, S. R. Weiss, and K. V. Holmes.** 2003. Conformational changes in the spike glycoprotein of murine coronavirus are induced at 37°C either by soluble murine CEACAM1 receptors or by pH 8. J. Virol. **77:**830–840.
55. **Zimmer, G., L. Budz, and G. Herrler.** 2001. Proteolytic activation of respiratory syncytial virus fusion protein. Cleavage at two furin consensus sequences. J. Biol. Chem. **276:**31642–31650.
56. **Zimmer, G., M. Rohn, G. P. McGregor, M. Schemann, K. K. Conzelmann, and G. Herrler.** 2003. Virokinin, a bioactive peptide of the tachykinin family, is released from the fusion protein of bovine respiratory syncytial virus. J. Biol. Chem. **278:**46854–46861.